Biogeosciences, 11, 269–280, 2014
www.biogeosciences.net/11/269/2014/
doi:10.5194/bg-11-269-2014

Biogeosciences Open Access

On the consistency of MODIS chlorophyll *a* products in the northern South China Sea

S. L. Shang[1,2], Q. Dong[2], C. M. Hu[3], G. Lin[1], Y. H. Li[1], and S. P. Shang[1,2]

[1]Key Laboratory of Underwater Acoustic Communication and Marine Information Technology (Xiamen University), Ministry of Education of China, Xiamen 361005, China
[2]Research and Development Center for Ocean Observation Technologies, Xiamen University, Xiamen 361005, China
[3]College of Marine Science, University of South Florida, 140 Seventh Ave. S., St. Petersburg, FL 33701, USA

Correspondence to: S. L. Shang (slshang@xmu.edu.cn)

Received: 10 April 2013 – Published in Biogeosciences Discuss.: 2 May 2013
Revised: 10 November 2013 – Accepted: 4 December 2013 – Published: 22 January 2014

Abstract. Chlorophyll *a* (Chl) concentrations derived from satellite measurements have been used in oceanographic research, for example to interpret eco-responses to environmental changes on global and regional scales. However, it is unclear how existing Chl products compare with each other in terms of accuracy and consistency in revealing temporal and spatial patterns, especially in the optically complex marginal seas. In this study, we examined three MODIS (Moderate Resolution Imaging Spectroradiometer) Chl data products that have been made available to the community by the US National Aeronautics and Space Administration (NASA) using community-accepted algorithms and default parameterization. These included the products derived from the OC3M (ocean chlorophyll three-band algorithm for MODIS), GSM (Garver–Siegel–Maritorena model) and GIOP (generalized inherent optical properties) algorithms. We compared their temporal variations and spatial distributions in the northern South China Sea. We found that the three products appeared to capture general features such as unique winter peaks at the Southeast Asian Time-series Study station (SEATS, 18° N, 116° E) and the Pearl River plume associated blooms in summer. Their absolute magnitudes, however, may be questionable in the coastal zones. Additional error statistics using field measured Chl as the truth demonstrated that the three MODIS Chl products may contain high degree of uncertainties in the study region. Root mean square error (RMSE) of the products from OC3M and GSM (on a log scale) was about 0.4 and average percentage error (ε) was $\sim 115\,\%$ (Chl between 0.05–10.41 mg m^{-3}, $n = 114$). GIOP with default parameterization led to higher errors ($\varepsilon = 329\,\%$). An attempt to tune the algorithms based on a local coastal-water bio-optical data set led to reduced errors for Chl retrievals, indicating the importance of local tuning of globally-optimized algorithms. Overall, this study points to the need of continuous improvements for algorithm development and parameterization for the coastal zones of the study region, where quantitative interpretation of the current Chl products requires extra caution.

1 Introduction

Chl *a* is the primary phytoplankton pigment for photosynthesis, whose concentration (hereafter abbreviated as Chl, mg m^{-3}) has been commonly used as a phytoplankton biomass index by oceanographers. Over the past three decades, an unprecedented view of the spatiotemporal pattern of Chl in the global ocean has been enabled by ocean color satellites such as CZCS (Coastal Zone Color Scanner), SeaWiFS (Sea-Viewing Wide Field-of-View Sensor) and MODIS (Moderate Resolution Imaging Spectroradiometer) (McClain, 2009). Based on these observations, a better understanding of the ecosystem health and carbon cycling associated with environmental changes at both global and regional scales has been achieved (e.g., Behrenfeld and Boss, 2006). Although the retrieval of Chl from satellite measurements is often problematic in optically complex coastal waters due to interference from non-pigment color matters, i.e., colored dissolved organic matter (CDOM) and detritus (e.g., Carder et al., 1989), and the use of optical indices

for phytoplankton pigmentation has become increasingly accepted (e.g., Cullen, 1982; Marra et al., 2007; Lee et al., 2011; Hirawake et al., 2011; Shang et al., 2011), Chl remains a basic, routinely sampled, and widely accepted oceanographic parameter for oceanographers.

Among the past and present ocean color sensors, MODIS is the major operational one at present and has been widely used by researchers to study global and regional oceanography. Previous evaluation of MODIS Chl demonstrated that MODIS Chl had moderately good agreement with measured Chl in oceanic waters (e.g., Zhang et al., 2006; Moore et al., 2009), while overestimation was often observed in turbid coastal waters (e.g., Darecki and Stramski, 2004; Magnuson et al., 2004; Werdell et al., 2009). Currently, there are three standard (operational) MODIS Chl data products provided by the US National Aeronautics and Space Administration (NASA) Ocean Biology Processing Group (OBPG, http://oceancolor.gsfc.nasa.gov), which are derived from MODIS remote sensing reflectance (R_{rs}, sr^{-1}) after atmosphere correction of MODIS measurements (http://oceancolor.gsfc.nasa.gov) over the ocean. The algorithms used to derive these products are the OC3M (ocean chlorophyll three-band algorithm for MODIS) blue/green band ratio algorithm (O'Reilly et al., 2000), the GSM (Garver–Siegel–Maritorena model) semi-analytical inversion algorithm (Maritorena et al., 2002), and the GIOP generalized IOPs (inherent optical properties) algorithm (Franz and Werdell, 2010; Werdell et al., 2013). Fundamentally, the OC3M empirical algorithm is different from the other two spectral optimization algorithms in two aspects (also see pp. 3–4 in the IOCCG report (2006) on the rationales of the various algorithms): (1) unlike the GSM and GIOP algorithms, the OC3M is not designed to differentiate Chl from other in-water constituents (Fig. 1). This is because, similar to Chl, both CDOM and detrital particles absorb blue light strongly, and the OC3M blue/green ratio algorithm cannot distinguish them explicitly. The GSM and GIOP are inherently similar in design. They are both based on a quantitative description of absorption and scattering properties of all optical components in the water, and the same semi-analytical reflectance model (Gordon, 1988) to describe how these properties (i.e., IOPs) determine the water's reflectance spectrum (i.e., spectral R_{rs}). Chl is then derived simultaneously with IOPs because Chl is a monotonous function of phytoplankton pigment absorption coefficient (a_{ph}). Both GSM and GIOP use mathematical optimization approaches to search for an optimal solution. The difference lies solely in the assumptions and parameterizations when modeling IOPs. For example, GSM uses fixed constants for the chlorophyll-specific phytoplankton pigment absorption coefficients (a^*_{ph}) while the default GIOP uses a^*_{ph} as a function of Chl (Bricaud et al., 1995). Their performance can therefore be influenced by the model parameterization (IOCCG, 2006; Huang et al., 2013). (2) The algorithm inputs (MODIS-derived R_{rs}) are also different. The inputs to the OC3M are R_{rs} at 443, 488, and 547 nm, while the inputs to the GSM and GIOP are R_{rs} data from all six MODIS bands. MODIS R_{rs} data in the blue bands (412 and 443 nm) are usually of low quality owing to the difficulties in atmospheric correction (e.g., Siegel et al., 2005; Bailey and Werdell, 2006), representing another important uncertainty source for all three algorithms.

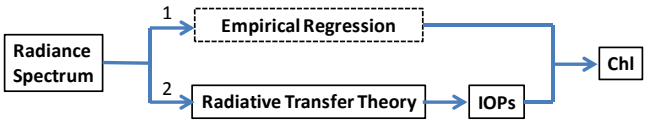

Fig. 1. Conceptual diagram of the OC3M (route 1), and the GSM and GIOP (route 2).

It has been well recognized that each algorithm has its own strengths and weaknesses (e.g., O'Reilly et al., 1998; Werdell, 2009). However, while an increasing number of users from the oceanographic community are using the various Chl products to interpret biogeochemical processes or temporal changes, the consistency between these Chl products is generally unknown, especially for marginal seas. Can certain spatiotemporal patterns be revealed by one Chl product but masked by another?

In this study, we attempted to address this question by using an extensive data set collected from a marginal sea. We chose the South China Sea (SCS) as the study region, not only because of the extensive effort in the past decade to collect field data but also because of its regional and global importance (e.g., Liu et al., 2002; Lin et al., 2003; Tang et al., 2004; Isoguchi et al., 2005; Tseng et al., 2005; Gan et al., 2009; Lin et al., 2010; Hong et al., 2011; Palacz et al., 2011; Xiu and Chai, 2011). Indeed, the SCS is the second largest marginal sea in the world. Data analysis will in particular be focused on the northern SCS (NSCS), where in situ data were collected for algorithm tuning and product evaluation (Fig. 2).

The study focused on three easily accessible standard (operational) MODIS Chl products (hereafter abbreviated as C_OC3M, C_GSM, and C_GIOP). Our goal is to demonstrate the consistency or discrepancy among the biogeochemical features in the SCS derived from these three easily accessible Chl products, to diagnose potential reasons of product inconsistency or high uncertainty, and to seek for potential solutions to reduce the product uncertainties. Specifically, the analysis was through (1) comparison of Chl spatiotemporal variations at the Southeast Asian Time-series Study station (SEATS), two typical coastal upwelling zones, and the Pearl River estuary; (2) evaluation of MODIS-derived R_{rs} and MODIS Chl products using field measured R_{rs} and Chl as the truth; and (3) regional tuning of the algorithms for the NSCS coastal zones based on a local bio-optics data set (R_{rs}, Chl, and a_{ph}).

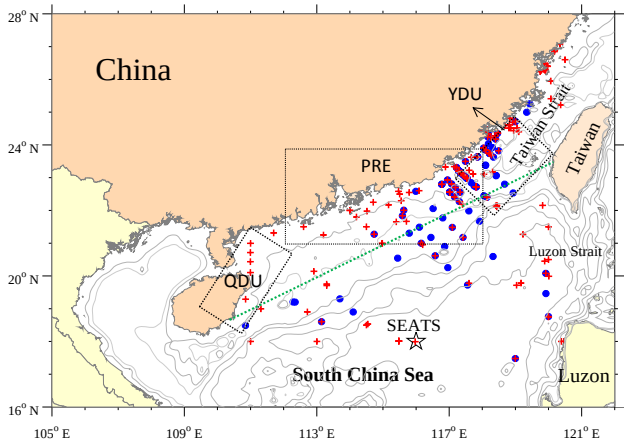

Fig. 2. Map of the study region. QDU and YDU refer to upwelling zones off Qiongdong and Yuedong boundaries; zones were defined following Jing et al. (2011). PRE refers to the Pearl River estuary, and SEATS refers to the Southeast Asian Time-series Study station (18° N, 116° E). Blue circles show the locations where concurrent MODIS R_{rs} data and in situ observed Chl were used for algorithm evaluations. Red crosses show the locations where concurrent field measured R_{rs} and Chl collected in the coastal waters were used for algorithm evaluations groups (from the green dotted line towards the shore) and were also used for further regional algorithm tuning.

2 Data and methods

2.1 MODIS standard Chl products for spatiotemporal analysis

Level 3 MODIS monthly mean and monthly climatology data products of Chl (C_OC3M, C_GSM, and C_GIOP) for 2002–2012 were obtained from the US NASA OBPG (http://oceancolor.gsfc.nasa.gov/) using the most recent updates in calibration and algorithms (reprocessing R2012.0), with a spatial resolution of approximately 4 km by 4 km. Data were extracted from the NSCS (105–121° E and 16–25° N) for further analysis of spatial and temporal patterns.

2.2 Data for algorithm evaluation and tuning

In order to help understand the reasons causing product inconsistency or uncertainty, we used both MODIS R_{rs} and in situ R_{rs} to test the algorithm performance. Regional tuning of algorithms, based on an in situ data set including R_{rs}, Chl and a_{ph}, was also conducted.

Daily MODIS R_{rs} data (level 2) at original resolution (approximately 1 km^2) were obtained from the same NASA group. MODIS data associated with the following quality control flags were discarded: atmospheric correction warning, large viewing angle, large sun angle, clouds, stray light, low water-leaving radiance, Chl algorithm failure, questionable navigation, and dark pixel.

For comparison between MODIS and in situ measurements, it is difficult to strictly follow the methods recommended by Bailey and Werdell (2006) due to heavy and frequent cloud cover over the study region. While a 3-by-3 pixel spatial window centered on the location of in situ measurement with the variance threshold of 0.15 was used, the temporal difference was relaxed to $< \pm 24$ h to allow for sufficient number of matchups for statistical analysis.

In situ R_{rs} Chl, and a_{ph} data were collected from targeted and opportunistic cruise surveys between 2003 and 2011 (Fig. 2), for which the measurement details can be found in Shang et al. (2011). Briefly, R_{rs} data were collected with an above-water GER 1500 spectroradiometer (Spectra Vista Corporation, USA), with a spectral resolution of 3.0 nm. Water samples were collected from a CTD rosette, from which Chl was measured fluorometrically (Lalli and Parsons, 1993), and a_{ph} was measured using a modified transmission–reflection (T–R) measurement method (Tassan and Ferrari, 1995; Dong et al., 2010).

In total, we compiled 114 pairs of daily MODIS R_{rs} and in situ Chl data (blue circles in Fig. 2), 87 pairs of daily MODIS R_{rs} and in situ R_{rs} data, and 192 groups of in situ R_{rs}, in situ Chl, and in situ a_{ph} data (red crosses in Fig. 2). Of these, 121 groups were collected from the coastal waters (red crosses within shoreline and the green dotted line in Fig. 2); these in situ data were also used in regional algorithm tuning. The entire data set covered a wide range of environmental settings, with Chl ranging from 0.03 mg m^{-3} in the oligotrophic NSCS to 51.15 mg m^{-3} in estuarine waters.

The three algorithms were implemented in IDL (interactive data language) to estimate Chl from the spectral R_{rs}. The OC3M parameterization was obtained from the NASA OBPG. The GSM algorithm, including its coding, was obtained from the International Ocean Color Coordination Group IOCCG, http://www.ioccg.org/groups/software.html, with necessary modifications to adjust for the wavelength shift from SeaWiFS to MODIS (S. Maritorena, personal communication, 2010). The GIOP algorithm with its default parameterization and the product failure flag set was taken from Brewin et al. (2012) and the NASA OBPG (http://oceancolor.gsfc.nasa.gov/WIKI/GIOPBaseline.html. Because no GIOP code was available, and considering that the GIOP and GSM algorithms were similar except in the IOPs parameterization, we implemented the GIOP algorithm by modifying the GSM code. In our GIOP code, the same optimization method (i.e., Levenberg–Marquardt) was used, and the OBPG suggested product failure conditions were applied to filter non-valid and unreliable retrievals. We tested our GIOP code by using the NASA Bio-Optical Marine Algorithm Data set (NOMAD) as input and found that the results were consistent with those produced by the NASA OBPG (http://oceancolor.gsfc.nasa.gov/cgi/giopval.cgi).

2.3 Error statistics

To assess the similarity or difference between measured and algorithm-derived parameters, four statistical indicators were calculated, following community-accepted standards (IOCCG, 2006; Moore et al., 2009). These indicators included the coefficient of determination (R^2), mean absolute percentage error (ε), bias (δ), and root mean square error (RMSE) in log scale, defined as follows:

$$\varepsilon = \frac{1}{n}\sum_{i=1}^{n}\frac{|y_i - x_i|}{x_i} \times 100\,\% \quad (1)$$

$$\delta = \frac{1}{n}\sum_{i=1}^{n}[\log_{10}(y_i) - \log_{10}(x_i)] \quad (2)$$

$$\mathrm{RMSE} = \sqrt{\frac{1}{n}\sum_{i=1}^{n}[\log_{10}(y_i) - \log_{10}(x_i)]^2} \quad (3)$$

where x represents the measured parameter and y represents the algorithm-derived parameter.

3 Results

Figure 3 shows MODIS Chl distributions in four months during spring, summer, fall, and winter. In general, all three Chl products showed similar seasonality and spatial distributions: (1) Chl is lower in spring and fall than in summer and winter; (2) Chl is lower in the offshore SCS (<0.1 – $\sim 0.1\,\mathrm{mg\,m^{-3}}$) than in nearshore waters ($\sim 1 - > 1\,\mathrm{mg\,m^{-3}}$); and (3) there is a large patch of elevated Chl in and to the west of the Luzon Strait in winter. However, some apparent differences among the three products were also found, as shown in Figs. 3 and 4. The seasonality in C-GIOP was not as apparent as in C_OC3M or C_GSM. While C_OC3M and C_GSM showed maxima in winter, C-GIOP showed rather flat temporal changes between summer and winter. Field observations showed high Chl during winter throughout the SCS basin (e.g., Chen, 2005; Ning et al., 2004), confirming the observed patterns in C_OC3M and C_GSM. In addition, within the Chl minimum season (i.e., spring), monthly variations for C_OC3M were quite different from those for C_GSM and C_GIOP. C_OC3M decreased consistently from March to May while the fluctuations of C_GSM and C_GIOP within this time frame were not distinct. Unfortunately no in situ data, either published or unpublished, could be found to help clarify which monthly variation patterns during spring were more convincing.

While Figs. 3 and 4 showed general patterns of the three Chl products, their consistency and discrepancy are detailed at several targeted locations, as shown below.

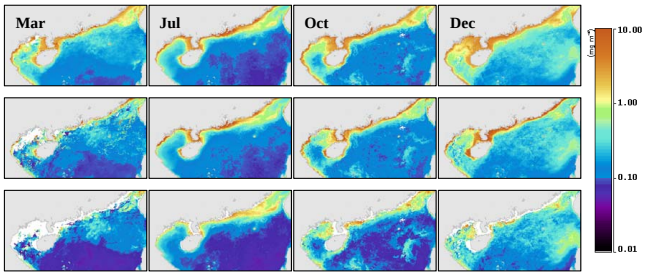

Fig. 3. Climatological monthly mean Chl in the northern South China Sea in March, July, October and December from three algorithms: (top) C_OC3M; (middle) C_GSM; (bottom) C_GIOP.

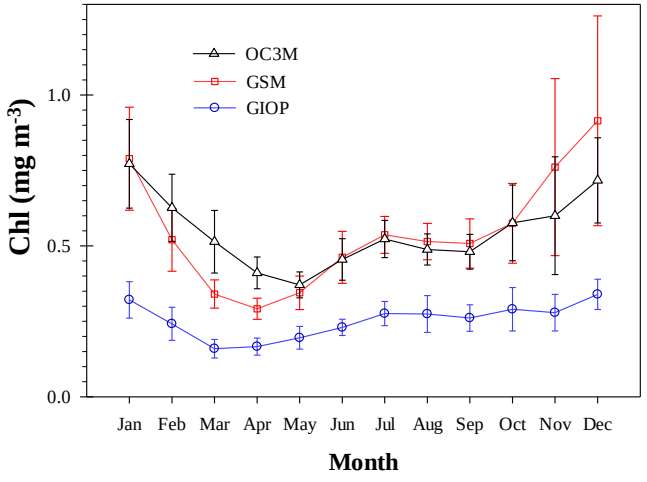

Fig. 4. Monthly climatology of MODIS Chl for the northern South China Sea (16–25° N, 105–121° E, the region depicted in Fig. 3).

3.1 SEATS

The SEATS (18° N, 116° E), located in the deep (> 3000 m) oligotrophic basin, was used to represent the SCS offshore waters. All products showed similar seasonality of Chl, i.e., elevated Chl in winter (Fig. 5a). This is consistent with in situ observations (Tseng et al., 2005). Very minor differences emerged in the detailed month-to-month and interannual variations (Fig. 5b). This is also illustrated by the strong correlation between C_GSM, C_GIOP and C_OC3M ($R > 0.8$, Fig. 6). When compared with the limited in situ data (red dots in Fig. 5b), differences were observed only for one data point in winter 2010 when both C_GSM and C_GIOP showed large departure from the in situ measurements. Note that this difference could be natural because one data point may not be representative of the mean state of the month. In general, all three Chl products showed consistent temporal patterns from this offshore SCS station.

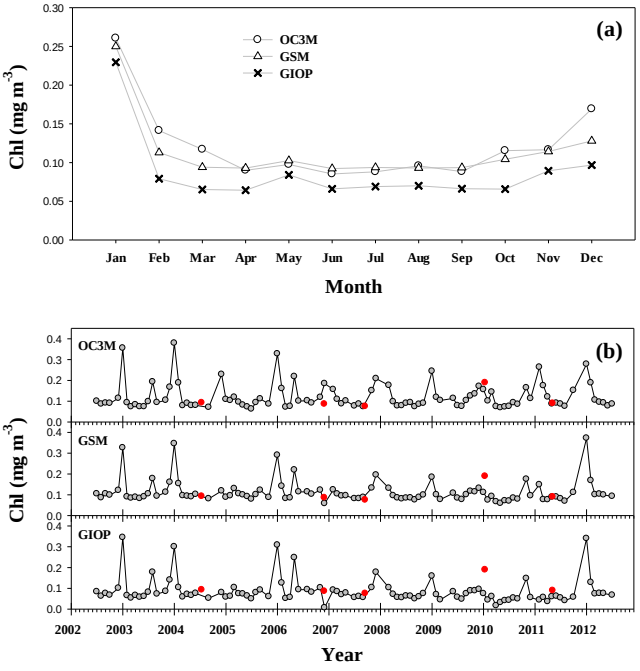

Fig. 5. Monthly climatology **(a)** and monthly variations **(b)** of MODIS Chl at SEATS. Red symbols refer to field measured Chl.

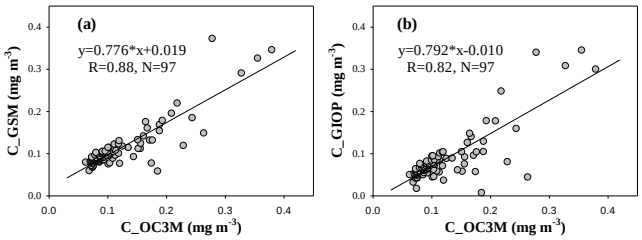

Fig. 6. Scatter plots showing the correlation between **(a)** C_OC3M and C_GSM; **(b)** C_OC3M and C_GIOP at SEATS.

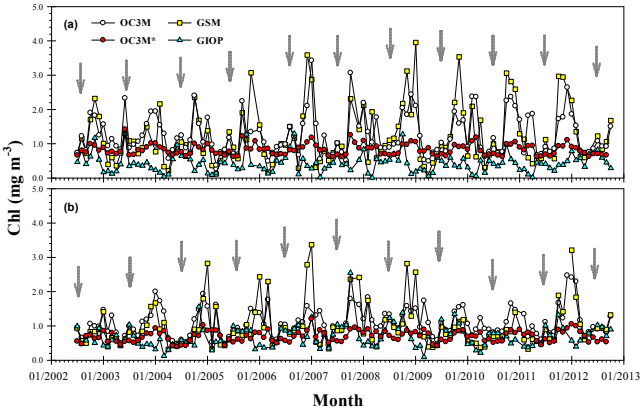

Fig. 7. Monthly variations of MODIS Chl in the Qiongdong **(a)** and Yuedong **(b)** upwelling zones; arrows indicate summer.

3.2 Summer upwelling zones

The NSCS is featured by upwelling (e.g., Xie et al., 2003; Gan et al., 2009; Hong et al., 2009; Jing et al., 2011). The consistency of the three Chl products was examined in two well-known coastal upwelling zones in summer, which are the upwelling zones off Qiongdong (QDU) and Yuedong (YDU) (see Fig. 2 for the locations).

Although the general patterns agreed with each other, the three products showed some differences in the mean monthly Chl extracted from the two zones (Fig. 7). C_OC3M and C_GSM appeared to have stronger seasonality (i.e., larger difference between annual maximum and annual minimum) than C_GIOP. More importantly, winter highs were more distinct than summer highs based on C_OC3M and C_GSM. This appeared contradictory from the seasonal patterns observed from very limited in situ measurements (e.g., Zhang et al., 1997), and from the knowledge that these two zones were short of nutrient supplies during winter (dry season) but were rich in nutrients owing to upwelling and land-based runoff during summer (wet season). This is possibly because Chl is overestimated in winter for C_OC3M and C_GSM. For C_OC3M, interference from non-phytoplankton matters (CDOM and detritus), which are commonly rich in these coastal waters, would cause Chl overestimation. For C_GSM, the globally optimized parameterization (Maritorena et al., 2002), such as Chl-specific absorption coefficient, may not be applicable in these coastal waters. This did not occur to C_GIOP possibly because data alongshore were filtered during data processing. Unfortunately, on the GIOP website there is no information on how the alongshore data are screened. One possibility is that those data fall under the preset product failure conditions (http://oceancolor.gsfc.nasa.gov/WIKI/GIOPBaseline.html).

3.3 Pearl River plume

There are two big rivers in the SCS, the Pearl River and the Mekong River. They contribute large amounts of fresh water as well as nutrients and other matters to the nearby ocean, thus having significant impact on the biogeochemistry of the SCS. Here we chose the Pearl River plume as an example to examine the time series derived from the three Chl data products.

Figure 8a shows the monthly climatology of C_OC3M, C_GSM and C_GIOP in the vicinity of the Pearl River estuary (PRE, 21–2° N, 112–118° E) in four months of different seasons. All three products consistently showed a distinct river plume extending eastward in summer.

To further compare the Chl products in nearshore waters, monthly climatology in January and July were extracted from waters shallower than 50 m. The monthly climatologies for the C_OC3M and C_GIOP were higher in July than in January (e.g., 3.30 mg m^{-3} versus 2.22 mg m^{-3}). This is consistent with the known seasonal patterns, i.e., higher Chl

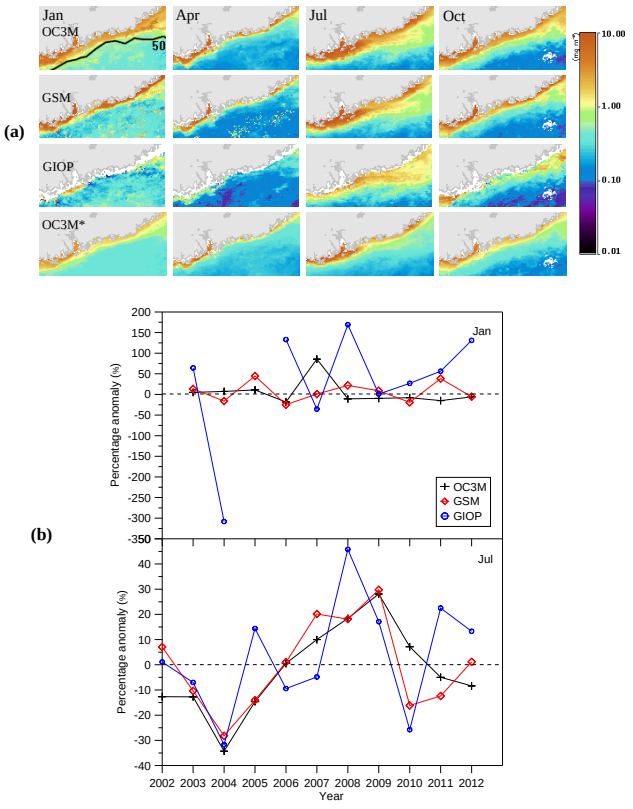

Fig. 8. (a) Monthly climatology of MODIS Chl in the vicinity of the Pearl River estuary in January, April, July and October. The isobath of 50 m is annotated on the January image of C_OC3M; **(b)** MODIS Chl anomaly (in percentage) in January and July of 2002–2012 for the nearshore waters of the Pearl River estuary (depth < 50 m).

in summer (wet season) than in winter (dry season) (e.g., Zhang, 2001). However, C_GSM was almost the same in January and July (3.42 mg m^{-3} versus 3.36 mg m^{-3}). This could be due to the improper parameterization of the GSM model, or due to high uncertainties in the MODIS R_{rs} data in the blue bands in nearshore waters.

The differences between the Chl products are further illustrated in the monthly anomaly patterns (Fig. 8b). Note that the monthly anomalies were calculated by simply deducing the monthly climatology from the monthly mean. In January, C_OC3M showed a strong positive anomaly in 2007, and C_GSM and C_GIOP appeared to have anomalies in the opposite directions. In July, the anomaly patterns of the three products were relatively similar to each other. A strong negative anomaly was found in 2004 in all three products, while the years of positive anomalies showed some discrepancy. Assuming that +25 % higher than climatology indicated a positive anomaly, a unique positive anomaly was found in 2009 for C_OC3M and C_GSM, while a > 25 % anomaly was found in 2008 for C_GIOP. Based on these observations, it could be inferred that summer blooms associated with river plumes and upwelling (e.g., Gan et al., 2010; Dai et al., 2008) were relatively weak in 2004. The bloom would however be inferred to be strong in 2009 if it was based on C_OC3M and C_GSM, or in 2008 if it was based on C_GIOP. Thus, without field-based validations (e.g., measured Chl, river discharges, nutrient fluxes, wind forcing, etc.), interpretation of the standard satellite-based Chl data products requires extra caution for nearshore waters of the NSCS. Algorithm tuning based on local data is thus advocated for these waters.

4 Discussion

4.1 Causes of the inconsistency

The above results showed consistent Chl patterns in the NSCS basin waters but large differences in upwelling zones and river plumes from the three products. In order to help diagnose the reasons of such similarity and discrepancy, in situ data were used to evaluate algorithm performance.

First, MODIS-derived R_{rs} data were used as the algorithm inputs to derive Chl, and then compared with the measured Chl. Figure 9 shows the evaluation results and the statistics are listed in Table 1. The average percentage errors all exceeded the desired level of accuracy for satellite-derived Chl (35 %, Bailey and Werdell, 2006) in this dynamic marginal sea. Most of the MODIS-derived Chl values were overestimated, as indicated by the positive δ. However, except for C_GIOP, MODIS-derived Chl agreed with in situ Chl reasonably well ($\varepsilon \sim 113$ % to 118 %, RMSE ~ 0.380 to 0.400, δ 0.069 to 0.145, see Table 1). The poorer performance of C_GIOP is due in part to its poor performance in shallow waters (< 50 m, see red dots in Fig. 9c; $\varepsilon = 441$ %, $\delta = 0.464$, see Table 1).

To test whether the discrepancy resulted from the algorithms or from uncertainties in the MODIS R_{rs}, the accuracy of MODIS R_{rs} was evaluated using in situ R_{rs} (Fig. 10). In general, MODIS R_{rs} agreed well with ground truth data except at 412 nm. This is consistent from other reported results (e.g., Siegel et al., 2005; Bailey and Werdell, 2006; Antoine et al., 2008; Dong, 2010). R^2 ranged between 0.72 and 0.86 and ε was < 26 % for bands 443, 488, 531 and 547 nm, while ε were 31 % and 49 % for 412 nm and 667 nm. Because the 443, 488, and 547 nm bands were used to estimate Chl in the OC3M algorithm, the relatively lower uncertainties in the MODIS R_{rs} in these bands suggest that C_OC3M would be influenced less by the MODIS R_{rs} uncertainties than the other two products, which used all six bands to estimate Chl.

The uncertainties introduced by the algorithms were further examined by using in situ R_{rs} as the algorithm input, with the derived Chl compared with the measured Chl. Results are shown in Table 1 and Fig. 11. When compared with the field measured Chl, Chl derived from in situ R_{rs} agreed better than Chl derived from MODIS R_{rs} because of the reduction in the R_{rs} uncertainties and because of the removal of the mismatch between satellite pixel size and in

Table 1. Error statistics between derived and in situ Chl.

Algorithm	R^2	ε (%)	RMSE	δ	N	n
MODIS R_{rs} derived (in situ Chl = 0.05–10.41 mg m^{-3}, mean = 0.87, std = 1.36)						
OC3M	0.39	118	0.380	0.145	114	114
OC3M*	0.40	63	0.290	0.015	114	114
GSM	0.35	113	0.400	0.069	114	112
GSM*	0.29	76	0.329	0.029	114	112
GIOP	0.23	329	0.600	0.340	114	111
GIOP*	0.32	111	0.396	0.081	114	110
MODIS R_{rs} derived (< 50 m) (Chl = 0.09–10.41 mg m^{-3}, mean = 1.27, std = 1.70)						
OC3M	0.32	155	0.433	0.225	64	64
OC3M*	0.32	75	0.330	0.012	64	64
GSM	0.28	147	0.438	0.163	64	63
GSM*	0.24	80	0.356	−0.002	64	63
GIOP	0.16	441	0.692	0.464	64	61
GIOP*	0.26	131	0.431	0.108	64	63
In situ R_{rs} derived (Chl = 0.03–51.15 mg m^{-3}, mean = 2.89,std = 6.63)						
OC3M	0.81	111	0.363	0.132	192	192
GSM	0.85	94	0.342	0.086	192	174
GIOP	0.13	256	0.548	0.163	192	160

* N is the number of R_{rs} data input, while n is the number of valid retrievals.

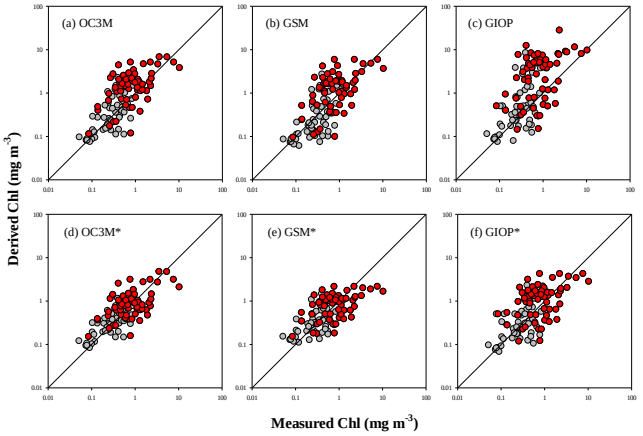

Fig. 9. Comparison between MODIS R_{rs} derived Chl and field measured Chl where MODIS Chl was derived using three algorithms and their tuned forms: **(a)** OC3M; **(b)** GSM; **(c)** GIOP; **(d)** tuned OC3M (OC3M*); **(e)** tuned GSM (GSM*); and **(f)** tuned GIOP (GIOP*). Red symbols refer to data collected from nearshore waters (depth < 50 m). Statistics of the algorithm performance are listed in Table 1.

situ sample size. Both OC3M and GSM performed well (R^2 ~ 0.81–0.85) although the error indices still exceeded the mission specifications (35 %). Similar to the above satellite-based analysis, GIOP showed lower R^2 (0.13) and higher error indices than the other two algorithms (e.g., ε ~ 256 %). The results suggest that the uncertainties in the three Chl products were mostly attributed to the inversion algorithms as opposed to imperfect atmospheric correction. However, it is unclear what caused the relatively poor performance of the GIOP algorithm in this marginal sea. Indeed, in an algorithm round-robin comparison, all 17 algorithms including GIOP were found to perform reasonably well in estimating Chl (Brewin et al., 2014). We speculate that the algorithm parameterization of GIOP requires a major tuning for the study region.

Thus, differences in the MODIS Chl data products appeared to have resulted mainly from the algorithm design in addressing the dependence of reflectance on the various in-water constituents. In the offshore (bottom depth >200 m) SCS where a_{ph}/a_t at 443 nm of the surface ocean ranges from 0.2 to 0.8 (a_t refers to the total absorption coefficient without water, $n = 119$; Shang, unpublished data), water's optical properties are predominantly driven by phytoplankton, or the optical properties of phytoplankton, CDOM, and detritus co-vary. Therefore, the three Chl products showed almost the same spatial and temporal patterns although their magnitudes varied slightly. In coastal upwelling zones and river plumes where the water is optically complex with significant amount of CDOM and detrital particles (both organic and mineral particles) (a_{dg}/a_t at 443 nm could be up to 0.97, where a_{dg} refers to the absorption coefficients of the sum of CDOM and detritus, Shang, unpublished data; also see Hong et al., 2005; Du et al., 2010), larger differences were found from the three Chl products. The OC3M empirical algorithm was not designed to differentiate Chl from other in-water constituents. The spectral optimization algorithms such as GSM and GIOP were designed to separate Chl from other in-water constituents, yet their performance was influenced by their fixed parameterization (IOCCG, 2006; Huang et al., 2013). For example, the parameterization for backscattering coefficients of particles (including both organic and mineral particles) may not reflect the truth in coastal waters rich in mineral particles. Failure in finding an optimal solution may be one reason for the pixel speckling in the C_GSM images and those masked nearshore pixels in the C_GIOP images (Fig. 8a). These failed pixels would cause a bias in calculating the mean and anomalies. Clearly, when time series data were analyzed, image series would need to be examined in order to identify these potential artifacts and to improve data interpretation.

4.2 Algorithm tuning

Based on the above analysis, in coastal waters the three Chl products are not consistent and might not reflect the truth. In order to solve the problem, we tuned the algorithms for coastal waters of the NSCS. In situ data for algorithm tuning were specifically collected from waters between the

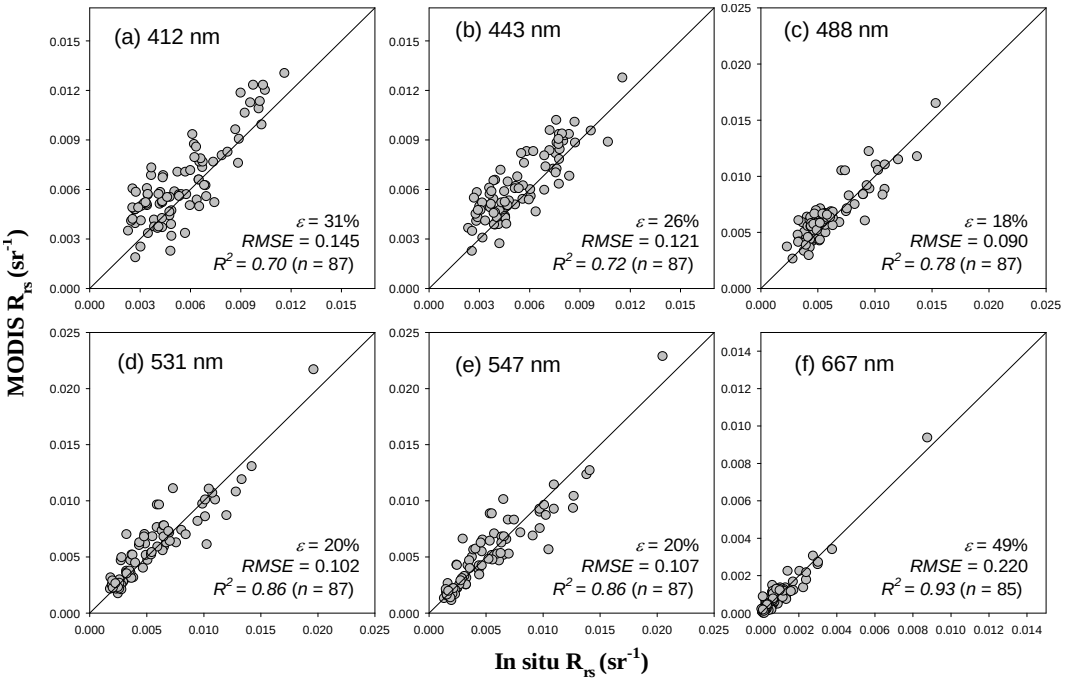

Fig. 10. Comparison between MODIS-derived R_{rs} and field measured R_{rs}.

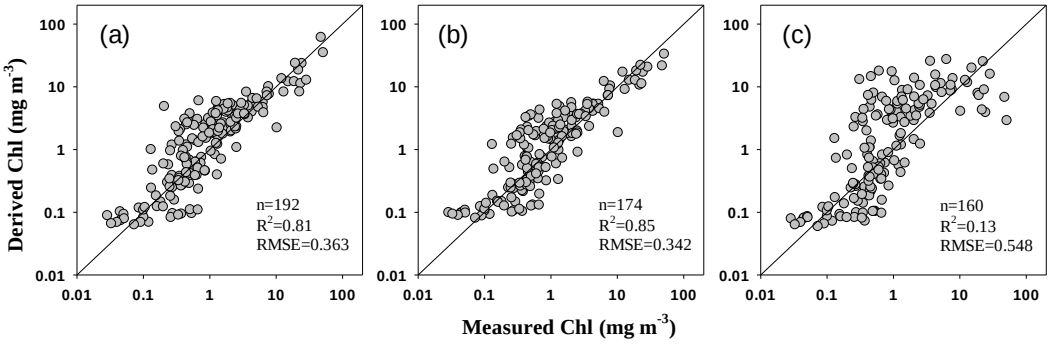

Fig. 11. Comparison between field measured Chl and in situ R_{rs} derived Chl using three algorithms: **(a)** OC3M; **(b)** GSM; **(c)** GIOP. Statistics of algorithm performance are listed in Table 1.

shoreline and the green dotted line in Fig. 2 (generally in the regions of PRE, QDU, and YDU). To facilitate data comparison, hereafter the regionally tuned algorithms are referred to as OC3M*, GSM*, and GIOP*.

The C_OC3M was derived from R_{rs} ratios as

$$\mathrm{Chl} = 10^{(c_0+c_1\times R_{\mathrm{ratio}}+c_2\times R_{\mathrm{ratio}}^2+c_3\times R_{\mathrm{ratio}}^3+c_4\times R_{\mathrm{ratio}}^4)} \quad (4)$$

$$R_{\mathrm{ratio}} = \log_{10}\left(\frac{\mathrm{Max}(R_{\mathrm{rs}}(443), R_{\mathrm{rs}}(488))}{R_{\mathrm{rs}}(547)}\right) \quad (5)$$

where c_0–c_4 are the algorithm coefficients determined from nonlinear regression between Chl and R_{rs} ratios. An in situ data set of R_{rs} and Chl ($n = 121$, sampled from coastal waters between the shoreline and the green dotted line in Fig. 2), was used to determine the algorithm coefficients, with results shown in Fig. 12 (blue dots and blue curve). For comparison, also shown in the figure, are the original NOMAD data set (http://seabass.gsfc.nasa.gov/, green crosses) and the default OC3M algorithm (green curve). Note that the local data covered almost the entire range of the NOMAD data set except for extremely clear waters. MODIS Chl calculated using the regionally tuned OC3M* were then compared to in situ Chl (Fig. 9d), which showed substantial improvements. The errors were almost halved (ε decreased from 126 % to 63 %, and RMSE decreased from 0.380 to 0.290; see Table 1).

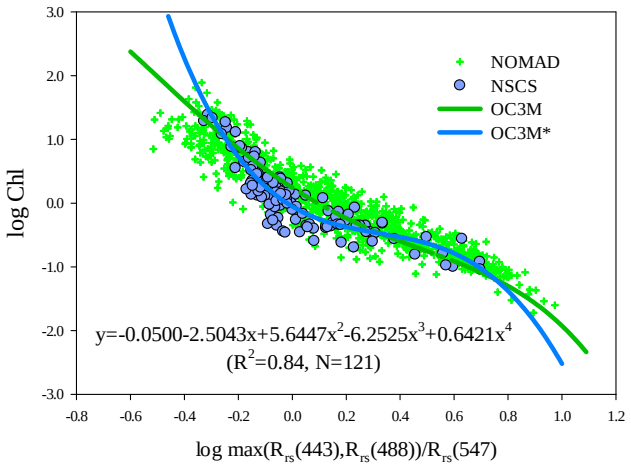

Fig. 12. Algorithm tuning for the OC3M band-ratio algorithm. All data were collected from in situ measurements. The green crosses and green curve are for the OC3M algorithm with default parameterization, while the blue dots represent local data collected from NSCS coastal waters. The blue curve is the locally tuned algorithm, with parameterization annotated on the figure.

In GSM and GIOP, $a_{\rm ph}$, $a_{\rm dg}$, and $b_{\rm bp}$ (particle backscattering coefficient) are modeled as

$$a_{\rm ph}(\lambda) = {\rm Chl} \times a^*_{\rm ph}(\lambda) \quad (6)$$

$$a_{\rm dg}(\lambda) = a(\lambda_0) \times \exp(-S_{\rm adg}(\lambda - \lambda_0)) \quad (7)$$

$$b_{\rm bp}(\lambda) = b_{\rm bp}(\lambda_0) \times (\frac{\lambda}{\lambda_0})^{-\eta} \quad (8)$$

where Chl, $a_{\rm dg}(\lambda_0)$ and $b_{\rm bp}(\lambda_0)$ are three scalar variables to be derived from a known $R_{\rm rs}$ spectrum via optimization. λ_0 is a reference wavelength and is generally set as 440 nm. In the models, $a^*_{\rm ph}$, $S_{\rm adg}$ (spectral slope of $a_{\rm dg}$) and η (power coefficient of $b_{\rm bp}$) can be tuned using local data. In the GSM parameterization, $S_{\rm adg}$ and η are optimized as 0.0206 nm^{-1} and 1.03373 for global waters, respectively; and $a^*_{\rm ph}$ is also optimized as a fixed spectrum for global waters, for example, $a_{\rm ph}(443) = {\rm Chl} \cdot 0.05582$ (Maritorena et al., 2002). In the default GIOP parameterization, $S_{\rm adg} = 0.018\,{\rm nm}^{-1}$, and η and $a^*_{\rm ph}$ are no longer fixed spectrum but using functional forms following that of the QAA Eq. (9), Lee et al. (2002, 2009) and Bricaud et al. (1995) Eq. (10), respectively:

$$\eta = 2.2 \times (1 - 1.2 \times e^{-0.9 \times \frac{r_{\rm rs}(443)}{r_{\rm rs}(555)}}), \quad (9)$$
$$(r_{\rm rs}(\lambda) = \frac{R_{\rm rs}(\lambda)}{0.52 + 1.7 \times R_{\rm rs}(\lambda)})$$

$$a^*_{\rm ph}(\lambda) = A(\lambda) \times {\rm Chl}^{-B(\lambda)}. \quad (10)$$

Table 2. Coefficients of $a^*_{\rm ph}(\lambda)$ for tuned GSM and GIOP.

Bands	GSM: $a^*_{\rm ph}(\lambda)$	GIOP: $a^*_{\rm ph}(\lambda) = A(\lambda)\ {\rm Chl}^{-B(\lambda)}$	
		A	B
412	0.0672	0.067	0.299
443	0.0754	0.071	0.281
488	0.0498	0.046	0.299
531	0.0176	0.019	0.292
547	0.0125	0.014	0.308
667	0.0264	0.027	0.209

The parameters of $a^*_{\rm ph}$, $S_{\rm adg}$, and η were tuned, and after trial and error we found that the following combination led to the lowest error budgets for Chl retrievals. (1) GSM*: $S_{\rm adg} = 0.018\,{\rm nm}^{-1}$ and η were calculated from Eq. (9). They were in fact the default setting of the GIOP; $a^*_{\rm ph}$ was re-derived based on an in situ $a_{\rm ph}$ and Chl data set collected in the target region, for example, now $a_{\rm ph}(443) = {\rm Chl} \cdot 0.0754$ (Table 2). (2) GIOP*: There was no change for $S_{\rm adg}$ and η while $a^*_{\rm ph}$ derived from regression based on the same in situ $a_{\rm ph}$ and Chl data set used for the GSM* (Table 2). In other words, for GIOP, only the coefficients of $a^*_{\rm ph}$ were tuned, while the GSM was tuned more thoroughly, with all three functions changed.

The regionally tuned algorithms were then used to calculate Chl using the MODIS $R_{\rm rs}$ as the algorithm inputs, and compared to concurrent in situ Chl. Evaluation results for the regionally tuned GSM* and GIOP* are shown in Fig. 9e and f and Table 1. Similar to OC3M*, the algorithms showed notable improvements over the original forms. For example, ε was reduced from 113 % to 76 % for the GSM* and 329 % to 111 % for the GIOP*. More substantial improvements were found for shallow waters (< 50 m, Table 1), where ε reduced from 441 % to 131 % for the GIOP*. Such improvements are better than those obtained from similar efforts for the Mediterranean Sea and western Canada coastal waters (D'Ortenzio et al., 2002; Komick et al., 2009). However, the errors are still higher than those from the OC3M*, suggesting more room for future algorithm development (Werdell et al., 2013).

Finally, based on the improved error statistics, OC3M* was chosen to re-derive the spatiotemporal patterns for the three coastal zones (Figs. 7 and 8a). In the QDU and YDU, the absolute magnitudes of Chl decreased while the seasonal patterns, i.e., peaking in winter, remained. Regardless of the tuning, it seems impossible to completely remove the interference of CDOM and detritus to the blue light absorption. However, in the PRE, the serious overestimation of Chl from the OC3M was partially corrected using the OC3M*.

5 Summary

Three MODIS Chl products are currently being used by the research community to address global and regional questions. These are derived from the OC3M, GSM, and GIOP algorithms. Yet their accuracy and consistency between each other are often unclear for marginal seas. Using a field data set collected from the NSCS, we evaluate the accuracy of the three MODIS Chl data products as well as their consistency in revealing spatial and temporal patterns under various scenarios.

The temporal changes and spatial distribution patterns in the three Chl data products differed mainly in optically complex nearshore waters, where certain spatiotemporal patterns revealed by one Chl product can be masked by another. In offshore SCS waters where optical properties are mostly dominated by phytoplankton, Chl seasonality and interannual changes derived from the three products were similar. This was mainly attributed to the algorithm design as opposed to the uncertainties in the input R_{rs}. The in situ validation (using in situ R_{rs} as input) showed RMSE errors > 0.3 in log scale and percentage errors > 90 % for all three Chl algorithms. While nearly identical statistical results were found for OC3M and GSM, GIOP showed significant deviation from the ground truth, possibly due to the incompatibility between its default parameterization and the optical properties of the NSCS. The three algorithms were then locally tuned. Tuning of the OC3M resulted in significant improvement in product accuracy for coastal waters, while the improvement from the tuned GSM and GIOP algorithms was not as profound.

Overall, for the study region of the NSCS it is suggested that (1) all three standard MODIS products yielded reasonable spatial and temporal patterns for the offshore basin waters; (2) current C_GIOP (with its default parameterization) is not proper for coastal water analysis because nearshore data are masked; (3) a clear specification of Chl product in oceanographic time-series studies would facilitate cross-study comparisons; and (4) regional tuning of the algorithms for coastal waters of the NSCS is necessary to reduce product uncertainty.

Acknowledgements. This work was supported jointly by NSF-China (#40976068), the National Basic Research Program of China (#2009CB421201), the Ministry of Science and Technology of China (#2013BAB04B00), and the University of South Florida. We thank the crew of the R/V *Dongfanghong II* and *Yanping II*, and J. Wu, X. Ma, X. Sui, W. Zhou, W. Wang, M. Yang, C. Du and G. Wei for their help in collecting in situ data. We also thank the NASA OBPG for providing MODIS data. We acknowledge the help from three anonymous reviewers who provided extensive comments and suggestions to improve this manuscript.

Edited by: K. Fennel

References

Antoine, D., d'Ortenzio, F., Hooker, S. B., Bécu, G., Gentili, B., Tailliez, D., and Scott, A. J.: Assessment of uncertainty in the ocean reflectance determined by three satellite ocean color sensors (MERIS, SeaWiFS and MODIS-A) at an offshore site in the Mediterranean Sea (BOUSSOLE project), J. Geophys. Res., 113, C07013, doi:10.1029/2007JC004472, 2008.

Bailey, S. W. and Werdell, P. J.: A multi-sensor approach for the on-orbit validation of ocean color satellite data products, Remote. Sens. Environ., 102, 12–23, 2006.

Behrenfeld, M. J. and Boss, E.: Beam attenuation and chlorophyll concentration as alternative optical indices of phytoplankton biomass, J. Mar. Res., 64, 431–451, 2006.

Brewin, R. J., Dall'Olmo, G., Sathyendranath, S., and Hardman-Mountford, N. J.: Particle backscattering as a function of chlorophyll and phytoplankton size structure in the open-ocean, Opt. Express, 20, 17632–17652, 2012.

Brewin, R. J. W., Sathyendranath, S., Müller, D., Brockmann, C., Deschamps, P.-Y., Devred, E., Doerffer, R., Fomferra, N., Franz, B., Grant, M., Groom, S., Horseman, A., Hu, C., Krasemann, H., Lee, Z. P., Maritorena, S., Mélin, F., Peters, M., Platt, T., Regner, P., Smyth, T., Steinmetz, F., Swinton, J., Werdell, J., and White III, G. N.: The Ocean Colour Climate Change Initiative: III. A round-robin comparison on in-water bio-optical algorithms, Remote. Sens. Environ., in press, doi:10.1016/j.rse.2013.09.016, 2014.

Bricaud, A., Babin, M., Morel, A., and Claustre, H.: Variability in the chlorophyll-specific absorption coefficients of natural phytoplankton: analysis and parameterization, J. Geophys. Res., 100, 13321–13332, 1995.

Carder, K. L., Steward, R. G., Harvey, G. R., and Ortner, P. B.: Marine humic and fulvic acids: their effects on remote sensing of ocean chlorophyll, Limnol. Oceanogr., 34, 68–81, 1989.

Chen, L.: Spatial and seasonal variations of nitrate-based new production and primary production in the South China Sea, Deep Sea Res. Pt. 1, 52, 319–340, 2005.

Cullen, J. J.: The deep chlorophyll maximum: comparing vertical profiles of chlorophyll a, Can. J. Fish. Aquat. Sci., 39, 791–803, 1982.

D'Ortenzio, F., Marullo, S., Ragni, M., Ribera d'Alcalà, M., and Santoleri, R.: Validation of empirical SeaWiFS algorithms for chlorophyll-a retrieval in the Mediterranean Sea: A case study for oligotrophic seas, Remote. Sens. Environ., 82, 79–94, 2002.

Darecki, M. and Stramski, D.: An evaluation of MODIS and SeaWiFS bio-optical algorithms in the Baltic Sea, Remote. Sens. Environ., 89, 326–350, 2004.

Dai, M., Zhai, W., Cai, W., Callahan, J., Huang, B., Shang, S., Huang, T., Li, X., Lu, Z., Chen, W., and Chen, Z.: Effects of an estuarine plume-associated bloom on the carbonate system in the lower reaches of the Pearl River estuary and the coastal zone of the northern South China Sea, Cont. Shelf Res., 28, 1416–1423, doi:10.1016/j.csr.2007.04.018, 2008.

Dong, Q.: Derivation of phytoplankton absorption properties from ocean color and its application, Ph.D. thesis, Xiamen University, China, 2010.

Du, C., Shang, S., Dong, Q., Hu, C., and Wu, J.: Characteristics of chromophoric dissolved organic matter in the nearshore waters of the western Taiwan Strait, Estuar. Coast. Shelf. S., 88, 350–356, doi:10.1016/j.ecss.2010.04.014, 2010.

Franz, B. A. and Werdell, P. J.: A generalized framework for modeling of inherent optical properties in ocean remote sensing applications, Ocean Optics XX, Anchorage, Alaska, 27th Sept.–1st Oct, 2010.

Gan, J. P., Li, L., Wang, D. X., and Guo, X. G.: Interaction of a river plume with coastal upwelling in the northeastern South China Sea, Cont. Shelf Res., 29, 728–740, doi:10.1016/j.csr.2008.12.002, 2009.

Gan, J. P., Lu, Z. M., Dai, M. H., Cheung, A. Y. Y., Liu, H. B., and Harrison, P.: Biological response to intensified upwelling and to a river plume in the northeastern South China Sea: A modeling study, J. Geophys. Res., 115, C09001, doi:10.1029/2009jc005569, 2010.

Gordon, H. R., Brown, O. B., Evans, R. H., Brown, J. W., Smith, R. C., Baker, K. S., and Clark, D. K.: A semianalytic radiance model of ocean color, J. Geophys. Res., 93, 10909–10924, 1988.

Hirawake, T., Takao, S., Horimoto, N., Ishimaru, T., Yamaguchi, Y., and Fukuchi, M.: A phytoplankton absorption-based primary productivity model for remote sensing in the Southern Ocean, Polar Biol., 34, 291–302, 2011.

Hong, H., Wu, J., Shang, S., and Hu, C.: Absorption and fluorescence of chromophoric dissolved organic matter in the Pearl River Estuary, South China, Mar. Chem., 97, 78–89, 2005.

Hong, H., Zhang, C., Shang, S., Huang, B., Li, Y., Li, X., and Zhang, S.: Interannual variability of summer coastal upwelling in the Taiwan Strait, Cont. Shelf Res., 29, 479–484, 2009.

Hong, H., Liu, X., Chiang, K.-P., Huang, B., Zhang, C., Hu, J., and Li, Y.: The coupling of temporal and spatial variations of chl *a* concentration and the East Asian monsoons in the southern Taiwan Strait, Cont. Shelf Res., 31, S37–S47, doi:10.1016/j.csr.2011.02.004, 2011.

Huang, S. H., Li, Y. H., Shang, S. P., and Shang S. L.: Impact of computational methods and spectral models on the retrieval of optical properties via spectral optimization, Opt. Express, 21: 6257–6273, 2013.

IOCCG: Remote Sensing of Inherent Optical Properties: Fundamentals, Tests of Algorithms, and Applications, in: Reports of the International Ocean-Colour Coordinating Group, No. 5, edited by: Lee, Z. P., IOCCG, Dartmouth, Canada, 126, 2006.

Isoguchi, O., Kawamura, H., and Ku-Kassim, K.-Y.: El Niño–related offshore phytoplankton bloom events around the Spratley Islands in the South China Sea, Geophys. Res. Lett., 32, L21603, doi:10.1029/2005GL024285, 2005.

Jing, Z., Qi, Y., and Du, Y.: Upwelling in the continental shelf of northern South China Sea associated with 1997–1998 El Niño, J. Geophys. Res., 116, C02033, doi:10.1029/2010JC006598, 2011.

Komick, N., Costa, M., and Gower, J.: Bio-optical algorithm evaluation for MODIS for western Canada coastal waters: An exploratory approach using in situ reflectance, Remote. Sens. Environ., 113, 794–804, 2009.

Lalli, C. M. and Parsons, T. R.: Biological Oceanography: An Introduction, Pergamon Press, Oxford, 1993.

Lee, Z. P., Carder, K. L., and Arnone, R. A.: Deriving inherent optical properties from water color: a multiband quasi-analytical algorithm for optically deep waters, Appl. Optics, 41, 5755–5772, 2002.

Lee, Z. P., Lubac, B., Werdell, J., and Arnone, R.: An Update of the Quasi-Analytical Algorithm (QAA_v5), International Ocean Color Group Software Report, 2009.

Lee, Z. P., Du, K., Voss, K. J., Zibordi, G., Lubac, B., Arnone, R., and Weidemann, A.: An inherent-optical-property-centered approach to correct the angular effects in water-leaving radiance, Appl. Optics, 50, 3155–3167, 2011.

Lin, I. I., Lien, C. C., Wu, C. R., Wong, G. T., Huang, C. W., and Chiang, T. L.: Enhanced primary production in the oligotrophic South China Sea by eddy injection in spring, Geophys. Res. Lett., 37, L16602, doi:10.1029/2010GL043872, 2010.

Lin, I., Liu, W. T., Wu, C.-C., Wong, G. T., Hu, C., Chen, Z., Liang, W.-D., Yang, Y., and Liu, K.-K.: New evidence for enhanced ocean primary production triggered by tropical cyclone, Geophys. Res. Lett., 30, 1718, doi:10.1029/2003GL017141, 2003.

Liu, K. K., Chao, S. Y., Shaw, P. T., Gong, G. C., Chen, C. C., and Tang, T.: Monsoon-forced chlorophyll distribution and primary production in the South China Sea: observations and a numerical study, Deep Sea Res. Pt. 1, 49, 1387–1412, 2002.

Magnuson, A., Harding, L. W., Mallonee, M. E., and Adolf, J. E.: Bio-optical model for Chesapeake Bay and the Middle Atlantic Bight, Estuar. Coast. Shelf. S., 61, 403–424, 2004.

Maritorena, S., Siegel, D. A., and Peterson, A. R.: Optimization of a semianalytical ocean color model for global-scale applications, Appl. Optics, 41, 2705–2714, 2002.

Marra, J., Trees, C. C., and O'Reilly, J. E.: Phytoplankton pigment absorption: a strong predictor of primary productivity in the surface ocean, Deep-Sea Res. I, 54, 155–163, 2007.

McClain, C. R.: A decade of satellite ocean color observations*, Annu Rev Mar Sci, 1, 19-42, 2009.

Moore, T. S., Campbell, J. W., and Dowell, M. D.: A class-based approach to characterizing and mapping the uncertainty of the MODIS ocean chlorophyll product, Remote. Sens. Environ., 113, 2424–2430, 2009.

Ning, X., Chai, F., Xue, H., Cai, Y., Liu, C., and Shi, J.: Physical-biological oceanographic coupling influencing phytoplankton and primary production in the South China Sea, J. Geophys. Res., 109, C10005, doi:10.1029/2004JC002365, 2004.

O'Reilly, J., Maritorena, S., Mitchell, B. G., Siegel, D., Carder, K. L., Garver, S., Kahru, M., and McClain, C.: Ocean color chlorophyll algorithms for SeaWiFS, J. Geophys. Res., 103, 24937–24953, 1998.

O'Reilly, J. E., Maritorena, S., Siegel, D., and O'Brien, M. C.: Ocean color chlorophyll a algorithms for SeaWiFS, OC2, and OC4: version 4, in: SeaWiFS postlaunch technical report series, volume 11, SeaWiFS postlaunch calibration and validation analyses, part 3, edited by: Hooker, S. B. and Firestone, E. R., Greenbelt, Maryland: NASA Goddard Space Flight Center, 9–23, 2000.

Palacz, A. P., Xue, H., Armbrecht, C., Zhang, C., and Chai, F.: Seasonal and inter-annual changes in the surface chlorophyll of the South China Sea, J. Geophys. Res., 116, C09015, doi:10.1029/2011JC007064, 2011.

Shang, S., Dong, Q., Lee, Z., Li, Y., Xie, Y., and Behrenfeld, M.: MODIS observed phytoplankton dynamics in the Taiwan Strait: an absorption-based analysis, Biogeosciences, 8, 841–850, doi:10.5194/bg-8-841-2011, 2011.

Shang, S., Li, L., Li, J., Li, Y., Lin, G., and Sun, J.: Phytoplankton bloom during the northeast monsoon in the Luzon Strait bordering the Kuroshio, Remote. Sens. Environ., 124, 38–48, 2012.

Siegel, D. A., Maritorena, S., Nelson, N. B., and Behrenfeld, M. J.: Independence and interdependencies among global ocean color

properties: Reassessing the bio-optical assumption, J. Geophys. Res., 110, C07011, doi:10.1029/2004JC002527, 2005.

Tang, D. L., Kawamura, H., and Guan, L.: Long-time observation of annual variation of Taiwan Strait upwelling in summer season, Monitoring of Changes Related to Natural and Manmade Hazards Using Space Technology, 33, 307–312, 2004.

Tassan, S. and Ferrari, G. M.: An alternative approach to absorption measurements of aquatic particles retained on filters, Limnol. Oceanogr., 40, 1358–1368, 1995.

Tseng, C. M., Wong, G. T. F., Lin, I. I., Wu, C. R., and Liu, K. K.: A unique seasonal pattern in phytoplankton biomass in low-latitude waters in the South China Sea, Geophys. Res. Lett., 32, L08608, doi:10.1029/2004GL022111, 2005.

Werdell, P. J.: Global bio-optical algorithms for ocean color satellite applications, AGU EOS Transactions, 90, p. 4, doi:10.1029/2009EO010005, 2009.

Werdell, P. J., Franz, B. A., Bailey, S. W., Feldman, G. C., Boss, E., Brando, V. E., Dowell, M., Hirata, T., Lavender, S. J., and Lee, Z.: Generalized ocean color inversion model for retrieving marine inherent optical properties, Appl. Optics, 52, 2019–2037, 2013.

Werdell, P. J., Bailey, S. W., Franz, B. A., Harding, Jr, L. W., Feldman, G. C., and McClain, C. R.: Regional and seasonal variability of chl *a* in Chesapeake Bay as observed by SeaWiFS and MODIS-Aqua, Remote Sens Environ, 113, 1319–1330, 2009.

Xie, S. P., Xie, Q., Wang, D., and Liu, W. T.: Summer upwelling in the South China Sea and its role in regional climate variations, J. Geophys. Res., 108, 3261, doi:10.1029/2003JC001867, 2003.

Xiu, P. and Chai, F.: Modeled biogeochemical responses to mesoscale eddies in the South China Sea, J. Geophys. Res., 116, C10006, doi:10.1029/2010JC006800, 2011.

Zhang, C. Y., Hu, C. M., Shang, S. L., Muller-Karger, F. E., Li, Y., Dai, M. H., Huang, B. Q., Ning, X. R., and Hong, H. S.: Bridging between SeaWiFS and MODIS for continuity of chlorophyll-a concentration assessments off Southeastern China, Remote. Sens. Environ., 102, 250–263, 2006.

Zhang, F., Yang, Y., and Huang, B.Q.: Impact of nutrients on the chlorophyll a concentration in the Taiwan Strait. In: Collection of Oceanography Research (7), edited by: Hong, H. S., Beijing, Ocean Press, 81–88, 1997. (in Chinese with English abstract).

Zhang, F.: Seasonal variation features of chlorophyll a content in Taiwan Strait, Journal of Oceanography in Taiwan Strait, 20, 314–318, 2001(in Chinese with English abstract).